Journal of Materials Chemistry A

PAPER

Cite this: J. Mater. Chem. A, 2016, 4, 16377

Ab initio prediction of a silicene and graphene heterostructure as an anode material for Li- and Na-ion batteries†

L. Shi, T. S. Zhao,* A. Xu and J. B. Xu

Received 15th August 2016
Accepted 21st September 2016

DOI: 10.1039/c6ta06976b

www.rsc.org/MaterialsA

Silicene has been predicted to be an extraordinary anode material for lithium-ion batteries with a large capacity and low lithium migration energy barriers, but the free-standing form of silicene is unstable, virtually requiring a substrate support. In this work, we propose to use graphene as a substrate and a protective layer of silicene, forming a van der Waals heterostructure of silicene and graphene (Si/G) to serve as a prospective anode material for lithium/sodium-ion batteries. *Ab initio* calculations show that the Si/G heterostructure not only preserves the silicene's large lithium/sodium capacity (487 mA h g^{-1}) and low lithium/sodium migration energy barriers (<0.4 eV for lithium and <0.3 eV for sodium), but also provides much larger lithium/sodium binding energies *via* a synergistic effect, which can effectively inhibit the formation of dendrites. Density of states results show that the Si/G heterostructure is metallic before and after lithium/sodium intercalation, ensuring a good electronic conductivity. In addition, the mechanical stiffness of the Si/G heterostructure is found to be larger than that of pristine silicene or graphene, which helps preserve the structural integrity and enhance the cycle performance.

1. Introduction

Due to the increasing demand for energy storage systems with large capacity, high rate capability, good cycle performance and low price, conventional lithium-ion batteries based on graphite anodes can no longer provide satisfactory performance.[1–3] Among all the explored candidates for the next-generation anode material, two-dimensional (2D) materials have attracted great attention recently for their unique structural properties.[4–10] The 2D structure can provide a large surface area to accommodate lithium atoms, and the loose packing between the 2D layers can alleviate the volume expansion and contraction caused by the intercalation and deintercalation of lithium atoms. On the other hand, sodium-ion batteries have been regarded as promising alternatives for lithium-ion batteries due to the abundance of the sodium element and their low price.[11–13] Similar to that of lithium-ion batteries, the 2D material is also a prospective choice for the anode material of sodium-ion batteries for the weak van der Waals interaction between layers, which can accommodate the large volume expansion caused by sodium intercalation and maintain the structural integrity.[14–18]

Silicene, the silicon analogue of graphene, has been predicted to be an excellent 2D anode material for lithium-ion batteries with large theoretical capacity and low lithium migration energy barriers.[19,20] However, the free-standing form of silicene is unstable, virtually requiring a substrate support. Most of the successfully synthesized silicenes are deposited on metal substrates like Ag(111) and Ir(111).[21–24] The strong interaction between the substrates and silicene perturbed the electronic structure of pristine silicene,[25,26] and may induce surface reconstruction.[27] As a consequence, the promising properties of pristine silicene as an anode material are lost. Recently, along with the development of nanotechnology, more and more van der Waals heterostructures composed of different 2D materials have been successfully fabricated and shown integrated properties of isolated materials.[28–31] It has been predicted that graphene can serve as a substrate for silicene in place of metal substrates.[32,33] Different from the metal substrates, the interaction between silicene and graphene is mainly van der Waals force, which can preserve the intrinsic properties of silicene. Moreover, the involvement of graphene is also expected to provide better mechanical properties and higher electronic conductivity, and protect the silicene from environmental contamination.[34,35]

In this work, we provide a comprehensive first principles investigation on the feasibility of using the heterostructure of silicene and graphene as the anode material for lithium-ion and sodium-ion batteries. The results show that the Si/G heterostructure can not only maintain silicene's large capacity and low

Department of Mechanical and Aerospace Engineering, The Hong Kong University of Science and Technology, Clear Water Bay, Kowloon, Hong Kong, China. E-mail: metzhao@ust.hk; Tel: +852 2358 8647

† Electronic supplementary information (ESI) available. See DOI: 10.1039/c6ta06976b

migration energy barriers for both lithium and sodium, but also provide stronger lithium/sodium adsorption, better mechanical stiffness and good structural stability during the discharge/charge process, making it an attractive choice for the anode material of lithium/sodium-ion batteries.

2. Computational methodology

All the calculations were performed using Quantum ESPRESSO software package,[36] with Perdew–Burke–Ernzerhof (PBE) generalized gradient approximation (GGA)[37] and the projector augmented-wave (PAW) method.[38] DFT-D2 correction was adopted to describe the van der Waals interaction.[39] The cut-off energy was set to be 78 Ry, and the k-point mesh was set to be <0.05 $Å^{-1}$. All the structures have been fully optimized with a force tolerance of 0.01 eV $Å^{-1}$. The charge population was calculated using the Bader charge analysis.[40,41]

A 2 × 2 supercell of silicene (16 silicon atoms) and a 3 × 3 supercell of graphene (36 carbon atoms) were used to construct the heterostructure, with a 20 Å vacuum layer spacing along the z-direction. The stacking stability (E_f) of silicene and graphene was evaluated by:[34]

$$E_f = \frac{(E_{Si} + E_G - E_{Si+G})}{n} \quad (1)$$

where E_f is the formation energy of the Si/G heterostructure; E_{Si}, E_G and E_{Si+G} are the total energies of silicene, graphene and the Si/G heterostructure, respectively. n is the total number of atoms in the Si/G heterostructure. The stiffness C_{2D} is defined as:[34]

$$C_{2D} = 2(E - E_0) \Big/ \left[A_0 \left(\frac{\Delta L}{L}\right)^2\right] \quad (2)$$

where E and E_0 are the total energies of the 2D structure with a lattice change and at an equilibrium state, A_0 is the area of the 2D structure at the equilibrium state, and ΔL and L are the lattice constant change and pristine lattice constant. The lattice constant change ($\Delta L/L$) is set to 3% in our study. The binding energies of lithium/sodium were calculated by:[5]

$$E_b = E_{substrate+M} - E_{substrate} - \mu_M \quad (3)$$

where $E_{substrate+M}$ is the total energy of the lithium or sodium (M) binding with the substrate (pristine silicene, graphene or Si/G heterostructure), $E_{substrate}$ is the total energy of the considered substrate, and μ_M is the chemical potential of metallic lithium or sodium. To evaluate the diffusion energy barriers of lithium/sodium, the nudged elastic band method (NEB) was adopted,[42] and five or eleven images were used depending on the migration length. The open circuit voltage was estimated by:[5]

$$OCV \approx [E_{Mx_1S} - E_{Mx_2S} + (x_2 - x_1)E_M]/(x_2 - x_1)e \quad (4)$$

where E_{Mx_1S}, E_{Mx_2S} and E_M mean the total energy of the substrate adsorbed with x_1 lithium/sodium atoms, the total energy of the substrate adsorbed with x_2 lithium/sodium atoms and the total energy of metallic lithium/sodium.

3. Results and discussion

3.1 Lithium/sodium adsorption and diffusion on pristine silicene and graphene

The optimized geometries of silicene and graphene are shown in Fig. 1. Silicene shows a slightly puckered honeycomb lattice with a Si–Si bond length of 2.27 Å, while graphene shows a flat honeycomb lattice with a C–C bond length of 1.43 Å, which is in good agreement with the literature.[19,20,34] To study the binding properties of lithium and sodium onto pristine silicene and graphene, four adsorption sites on silicene (A1, A2, A3, and A4 as shown in Fig. 1(a1)) and three adsorption sites on graphene (B1, B2, and B3 as shown in Fig. 1(b1)) were chosen. The binding energies and corresponding charge transfer are listed in Table S1.† For silicene, the A1 site shows the largest binding energy of −0.87 eV for lithium and −0.84 eV for sodium, accompanied by +0.88 |e| and +0.86 |e| charge transfer from lithium/sodium to silicene, respectively. For graphene, the B1 site shows the largest binding energy for the cases of both lithium and sodium, but the binding energies are quite small. For lithium, the binding energy is only −0.02 eV, and for sodium, the binding energy is a positive value of +0.03 eV. This weak adsorption of lithium/sodium onto graphene is consistent with previous reports.[43–45] Vacancies or doping is necessary to enhance the adsorption when using graphene as an anode material for lithium/sodium-ion batteries.[44,45]

We then studied the diffusion properties of lithium/sodium on the surface of silicene and graphene, and the results are shown in Fig. 2. For silicene, both lithium and sodium prefer to first migrate to the top of the silicon atom at a lower position, and then migrate to the other hollow site, which agrees well with the literature.[19] The migration energy barrier is 0.35 eV for lithium and 0.23 eV for sodium. For graphene, the optimized migration path for both lithium and sodium is directly across the bridge site of two carbon atoms, with a migration energy barrier of 0.38 eV for lithium and 0.14 eV for sodium.

3.2 Lithium/sodium adsorption and diffusion in the heterostructure of silicene and graphene

A 2 × 2 supercell of silicene (16 Si atoms) and a 3 × 3 supercell of graphene (36 C atoms) were used to construct the Si/G heterostructure as shown in Fig. 3. The lattice mismatch between the silicene and graphene on both x and y directions is below

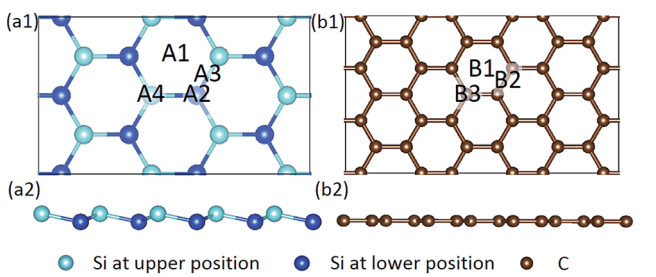

Fig. 1 Optimized structure and chosen adsorption sites of (a) silicene and (b) graphene.

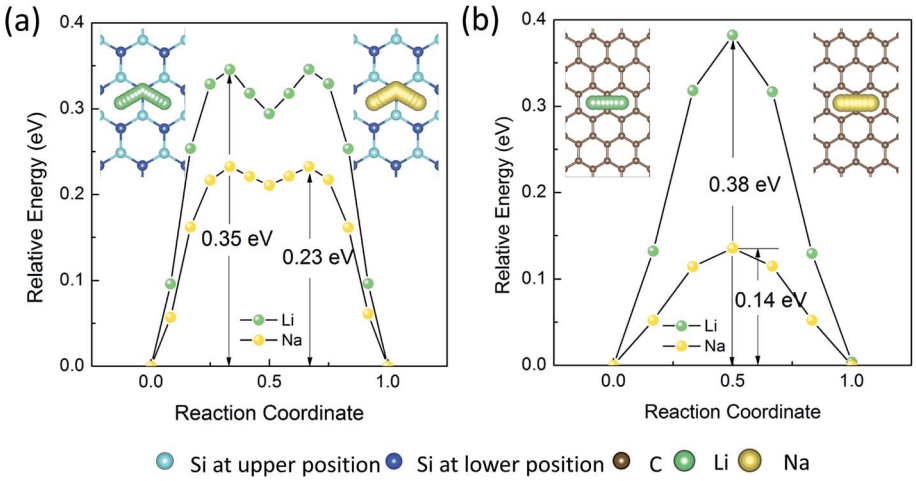

Fig. 2 Migration path and energy barrier of lithium and sodium on (a) silicene and (b) graphene.

4%. After geometrical optimization, the interlayer spacing between silicene and graphene is about 3.53 Å, and the calculated formation energy of the Si/G heterostructure is 14.16 meV per atom (46.02 meV per Si atom), which agrees well with previous calculation results.[32,33] The density of states for the Si/G heterostructure in Fig. 3(c) shows that the hybrid material is metallic, which can provide good electronic conductivity when used as an anode in lithium/sodium-ion batteries. The mechanical stiffness of pristine silicene and graphene and the heterostructure of silicene and graphene are calculated according to eqn (2). The obtained stiffness is 65.78 N m^{-1} for silicene, 292.78 N m^{-1} for graphene, and 383.45 N m^{-1} for the Si/G heterostructure. The higher mechanical stiffness of the Si/G heterostructure can help preserve the structural integrity of the anode and contribute to better cycle performance.

To study the binding of lithium and sodium in this Si/G heterostructure, three situations were considered: (1) lithium/sodium adsorption on the outside surface of silicene (Li/Si/G and Na/Si/G), (2) lithium/sodium adsorption between the silicene and graphene (Si/Li/G and Si/Na/G), and (3) lithium/sodium adsorption on the outside surface of graphene (Si/G/Li and Si/G/Na). For the first two situations, five symmetrically different adsorption sites were chosen as shown in Fig. 3(a), and for the last situation, seven symmetrically different adsorption sites were chosen as shown in Fig. 3(b). The detailed calculation results on the binding energy, charge transfer and equilibrium interlayer spacing after lithium/sodium adsorption are listed in

Table 1 Mean adsorption energy, charge transfer and equilibrium interlayer spacing for lithium and sodium adsorbed at the top/middle/bottom of the Si/G heterostructure

	Li/Si/G	Na/Si/G	Si/Li/G	Si/Na/G	Si/G/Li	Si/G/Na
$\overline{E_b}$ (eV)	−1.03	−0.96	−1.52	−1.30	−0.19	−0.12
$\overline{\Delta Q_{Li/Na}}$ (|e|)	+0.88	+0.86	+0.86	+0.84	+0.91	+0.93
$\overline{D_{Si-C}}$ (Å)	3.53	3.52	3.69	4.03	3.69	3.68

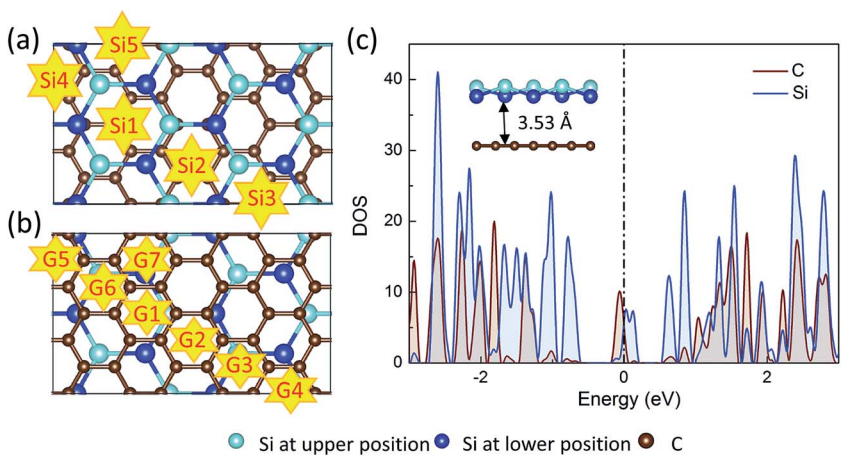

Fig. 3 The Si/G heterostructure geometry and chosen adsorption sites from the (a) top and (b) bottom view. (c) The density of states of the Si/G heterostructure.

Tables S2–S4.† It is found that for each situation, the difference among different adsorption sites is quite small (<0.06 eV for binding energy, <0.03 |e| for charge transfer and <0.04 Å for interlayer spacing). The mean binding energy, charge transfer and equilibrium interlayer spacing for lithium/sodium adsorbed in the abovementioned three situations are listed in Table 1. The binding energies for lithium/sodium adsorbed between silicene and graphene are shown to be the largest (−1.52 eV for lithium and −1.30 eV for sodium), much larger than those on pristine silicene or graphene. Thus during the charge process, lithium/sodium atoms will prefer to occupy the interlayer spacing between silicene and graphene first. More interestingly, for the situations when lithium/sodium is adsorbed on the outside surface of silicene or graphene, the binding energies are also higher than those on pristine silicene or graphene, and both the binding energies of lithium and sodium adsorption onto the outside surface of graphene become negative. The larger binding energies provided by the Si/G heterostructure can effectively prevent the clustering of lithium/sodium atoms and thus inhibit dendrite growth.

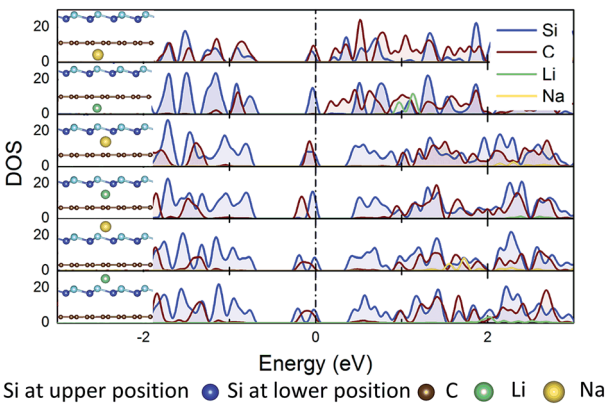

Fig. 4 Density of states of the Si/G heterostructure adsorbed with lithium and sodium on different sites.

From Bader charge analysis, lithium/sodium loses most of its electrons to the Si/G heterostructure and exists in the form of cations in all the situations considered. The density of states for Li/Si/G, Na/Si/G, Si/Li/G, Si/Na/G, Si/G/Li and Si/G/Na is plotted in Fig. 4. For all the adsorption situations, the Si/G heterostructure can preserve its metallic feature well, which ensures high electronic conductivity during the lithium/sodium intercalation process.

Then we studied the diffusion properties of lithium and sodium in the Si/G heterostructure. Also, the three situations mentioned above were considered. The calculation results are shown in Fig. 5. For the Li/Na diffusion on the outside surface of silicene, the migration energy barriers for lithium (0.36 eV) and sodium (0.22 eV) are similar to those on pristine silicene. Both lithium and sodium prefer to migrate to the silicon atom at the lower position first, which is in accordance with the pristine silicene situation. For the Li/Na diffusion between silicene and graphene, the situation is a bit different. For lithium, the migration energy barrier (0.37 eV) is between the value for pristine silicene (0.35 eV) and pristine graphene (0.38 eV), and lithium will migrate to the silicon atom at the higher position first, which is equivalent with the situation on pristine silicene. While for the sodium atom, the migration energy barrier (0.30 eV) is higher than both the migration energy barriers on pristine silicene (0.23 eV) and pristine graphene (0.14 eV), and the sodium atom prefers to migrate directly across the Si–Si/C–C bridge site. This is caused by the larger size of the sodium atom, which will induce stronger structural deformation when it is inserted into the interlayer spacing between silicene and graphene. For Li/Na diffusion on the outside surface of graphene, the migration energy barriers of lithium (0.40 eV) and sodium (0.19 eV) are also close to that on pristine graphene. From the above results, for all the situations considered, the diffusion energy barriers are lower than 0.40 eV for lithium and lower than 0.30 eV for sodium, which ensures good rate capability when used as the anode material for lithium/sodium-ion batteries.

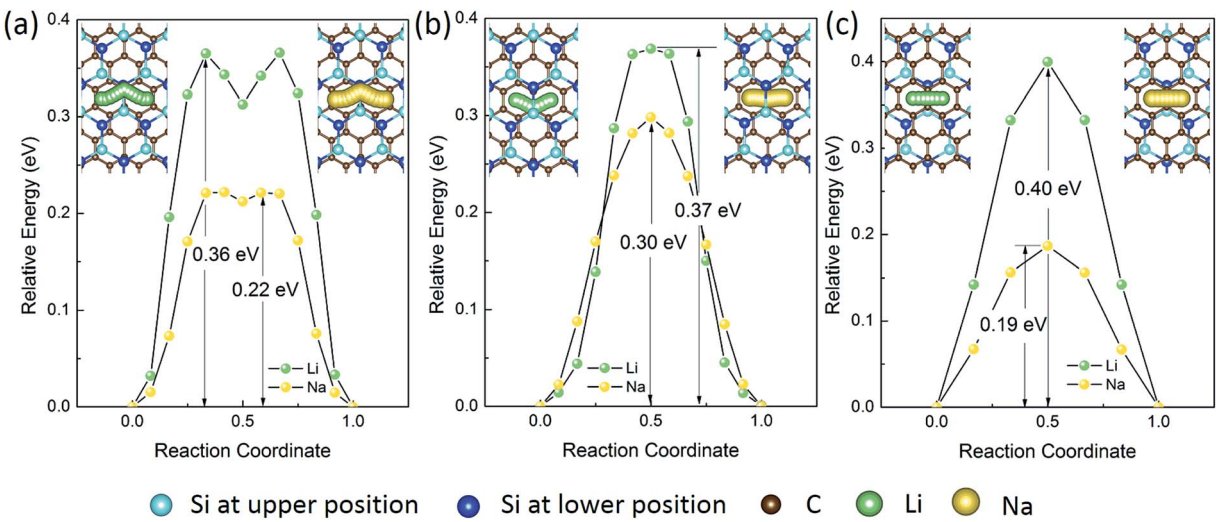

Fig. 5 Diffusion of lithium/sodium at the (a) top (b) middle and (c) bottom of the Si/G heterostructure.

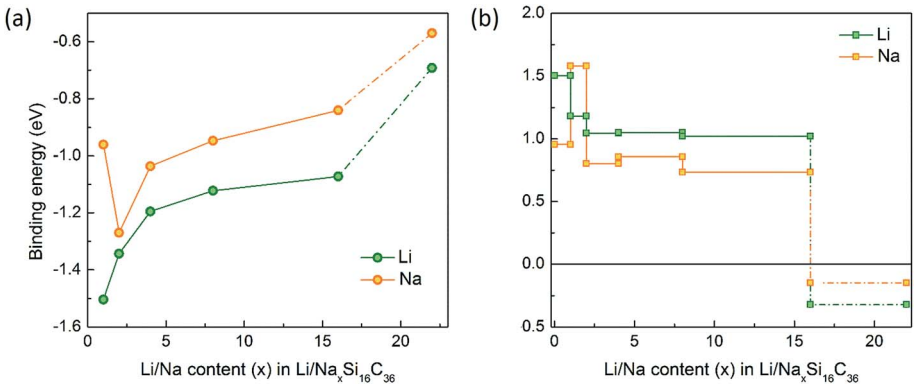

Fig. 6 (a) The binding energy of lithium and sodium adsorption onto the Si/G heterostructure at different Li/Na concentrations. (b) The calculated voltage profiles along with the lithiation/sodiation process.

3.3 Electrochemical properties of the lithium/sodium adsorbed Si/G heterostructure

In this section, we studied the adsorption behavior of the lithium/sodium atom in the Si/G heterostructure at different concentrations ($M_xSi_{16}C_{36}$, M = Li, Na, $x = 1$, 2, 4, 8, 16, and 22). The arrangement of Li and Na at different ion concentrations after geometrical optimization is shown in Fig. S1.† The binding energies for lithium and sodium at different concentrations are shown in Fig. 6(a). For all the concentrations considered, the binding energies for both lithium and sodium are negative. When the lithium/sodium concentration reaches $M_{22}Si_{16}C_{36}$, all the surfaces are fully adsorbed with lithium/sodium atoms, and the binding energies are still lower than −0.65 eV for lithium and lower than −0.55 eV for sodium. This strong adsorption at higher concentrations of lithium and sodium can effectively anchor the lithium and sodium atoms in the Si/G heterostructure and prevent them from clustering during the discharge/charge process.

Then we estimated the open-circuit voltage (OCV) during the lithiation/sodiation process using eqn (4). As shown in Fig. 6(b), for both lithium and sodium, the OCV becomes negative when the concentration reaches $M_{22}Si_{16}C_{36}$. Thus the highest concentration for both lithium and sodium intercalation during the charge process is $M_{16}Si_{16}C_{36}$, corresponding to a capacity of 487 mA h g^{-1}, with the outside surface of silicene and the interlayer spacing between silicene and graphene being fully adsorbed with lithium/sodium atoms. The calculated average OCV for the Si/G heterostructure is 1.07 V when used as the anode of lithium-ion batteries, and 0.84 V when used as the anode of sodium-ion batteries. These moderate OCVs can provide high energy density and at the same time effectively suppress dendrite growth. The interlayer spacing change during the lithium/sodium intercalation process is shown in Fig. S2.† It can be found that for lithium, the interlayer spacing expansion is about 20% during the intercalation process, and for sodium, the interlayer spacing expansion is about 40%. The moderate interlayer spacing expansion can help maintain the structural integrity during the discharge/charge process.

4. Conclusion

In this paper, we provide a comprehensive exploration on the feasibility of using the heterostructure of silicene and graphene as the anode material for lithium-ion and sodium-ion batteries. Graphene can serve as a substrate for silicene without perturbing its electronic structure as well as a protective layer to separate the silicene from environmental contamination. The calculation results show that the Si/G heterostructure can provide large adsorption energies and low migration energy barriers for both lithium and sodium. The theoretical capacity for both lithium and sodium is predicted to be as high as 487 mA h g^{-1}. The average open circuit potential is calculated to be 1.07 V for lithium and 0.84 V for sodium, which can provide large energy density and at the same time prevent dendrite growth. The mechanical stiffness of the heterostructure is higher than that of the pristine ones, ensuring good structural stability and cycle performance.

Acknowledgements

The work described in this paper was fully supported by a grant from the Research Grants Council of the Hong Kong Special Administrative Region, China (Project No. 16213414).

References

1 Y. G. Guo, J. S. Hu and L. J. Wan, *Adv. Mater.*, 2008, **20**, 2878–2887.
2 L. Ji, L. Zhan, M. Alcoutlabi and X. Zhang, *Energy Environ. Sci.*, 2011, **4**, 2682–2699.
3 W. Xu, J. Wang, F. Ding, X. Chen, E. Nasybulin, Y. Zhang and J. G. Zhang, *Energy Environ. Sci.*, 2014, **7**, 513–537.
4 Y. Jing, Z. Zhou, C. R. Cabrera and Z. Chen, *J. Mater. Chem. A*, 2014, **2**, 12104–12122.
5 Y. Jing, Z. Zhou, C. R. Cabrera and Z. Chen, *J. Phys. Chem. C*, 2013, **117**, 25409–25413.
6 M. Naguib, J. Halim, J. Lu, K. M. Cook, L. Hultman, Y. Gogotsi and M. W. Barsoum, *J. Am. Chem. Soc.*, 2013, **135**, 15966–15969.

7 Y. Xie, Y. Dall'Agnese, M. Naguib, Y. Gogotsi, M. W. Barsoum, H. L. Zhuang and P. R. Kent, *ACS Nano*, 2014, **8**, 9606–9615.

8 W. Li, Y. Yang, G. Zhang and Y. W. Zhang, *Nano Lett.*, 2015, **15**, 1691–1697.

9 H. R. Jiang, Z. Lu, M. C. Wu, F. Ciucci and T. S. Zhao, *Nano Energy*, 2016, **23**, 97–104.

10 Q. Tang, Z. Zhou and P. Shen, *J. Am. Chem. Soc.*, 2012, **134**, 16909–16916.

11 M. D. Slater, D. Kim, E. Lee and C. S. Johnson, *Adv. Funct. Mater.*, 2013, **23**, 947–958.

12 H. Pan, Y. S. Hu and L. Chen, *Energy Environ. Sci.*, 2013, **6**, 2338–2360.

13 N. Yabuuchi, K. Kubota, M. Dahbi and S. Komaba, *Chem. Rev.*, 2014, **114**, 11636–11682.

14 E. Yang, H. Ji and Y. Jung, *J. Phys. Chem. C*, 2015, **119**, 26374–26380.

15 E. Yang, H. Ji, J. Kim, H. Kim and Y. Jung, *Phys. Chem. Chem. Phys.*, 2015, **17**, 5000–5005.

16 Y. X. Yu, *J. Phys. Chem. C*, 2016, **120**, 5288–5296.

17 V. V. Kulish, O. I. Malyi, C. Persson and P. Wu, *Phys. Chem. Chem. Phys.*, 2015, **17**, 13921–13928.

18 L. Shi, T. S. Zhao, A. Xu and J. B. Xu, *Science Bulletin*, 2016, **61**, 1138–1144.

19 G. A. Tritsaris, E. Kaxiras, S. Meng and E. Wang, *Nano Lett.*, 2013, **13**, 2258–2263.

20 S. M. Seyed-Talebi, I. Kazeminezhad and J. Beheshtian, *Phys. Chem. Chem. Phys.*, 2015, **17**, 29689–29696.

21 P. Vogt, P. De Padova, C. Quaresima, J. Avila, E. Frantzeskakis, M. C. Asensio, A. Resta, B. Ealet and G. Le Lay, *Phys. Rev. Lett.*, 2012, **108**, 155501.

22 D. Tsoutsou, E. Xenogiannopoulou, E. Golias, P. Tsipas and A. Dimoulas, *Appl. Phys. Lett.*, 2013, **103**, 231604.

23 L. Meng, Y. Wang, L. Zhang, S. Du, R. Wu, L. Li, Y. Zhang, G. Li, H. Zhou, W. A. Hofer and H. J. Gao, *Nano Lett.*, 2013, **13**, 685–690.

24 A. Fleurence, R. Friedlein, T. Ozaki, H. Kawai, Y. Wang and Y. Yamada-Takamura, *Phys. Rev. Lett.*, 2012, **108**, 245501.

25 C. L. Lin, R. Arafune, K. Kawahara, M. Kanno, N. Tsukahara, E. Minamitani, Y. Kim, M. Kawai and N. Takagi, *Phys. Rev. Lett.*, 2013, **110**, 076801.

26 S. Cahangirov, M. Audiffred, P. Tang, A. Iacomino, W. Duan, G. Merino and A. Rubio, *Phys. Rev. B: Condens. Matter Mater. Phys.*, 2013, **88**, 035432.

27 S. Cahangirov, M. Topsakal, E. Aktürk, H. Şahin and S. Ciraci, *Phys. Rev. Lett.*, 2009, **102**, 236804.

28 A. K. Geim and I. V. Grigorieva, *Nature*, 2013, **499**, 419–425.

29 Y. Liu, N. O. Weiss, X. Duan, H. C. Cheng, Y. Huang and X. Duan, *Nature Reviews Materials*, 2016, **1**, 6042.

30 T. Niu and A. Li, *Prog. Surf. Sci.*, 2015, **90**, 21–45.

31 H. Wang, F. Liu, W. Fu, Z. Fang, W. Zhou and Z. Liu, *Nanoscale*, 2014, **6**, 12250–12272.

32 Y. Cai, C. P. Chuu, C. M. Wei and M. Y. Chou, *Phys. Rev. B: Condens. Matter Mater. Phys.*, 2013, **88**, 245408.

33 B. Liu, J. A. Baimova, C. D. Reddy, A. W. K. Law, S. V. Dmitriev, H. Wu and K. Zhou, *ACS Appl. Mater. Interfaces*, 2014, **6**, 18180–18188.

34 G. C. Guo, D. Wang, X. L. Wei, Q. Zhang, H. Liu, W. M. Lau and L. M. Liu, *J. Phys. Chem. Lett.*, 2015, **6**, 5002–5008.

35 J. Sun, H. W. Lee, M. Pasta, H. Yuan, G. Zheng, Y. Sun, Y. Li and Y. Cui, *Nat. Nanotechnol.*, 2015, **10**, 980–985.

36 P. Giannozzi, S. Baroni, N. Bonini, M. Calandra, R. Car, C. Cavazzoni, D. Ceresoli, G. L. Chiarotti, M. Cococcioni, I. Dabo and A. Dal Corso, *J. Phys.: Condens. Matter*, 2009, **21**, 395502.

37 J. P. Perdew, K. Burke and M. Ernzerhof, *Phys. Rev. Lett.*, 1996, **77**, 3865.

38 P. E. Blöchl, *Phys. Rev. B: Condens. Matter Mater. Phys.*, 1994, **50**, 17953.

39 S. Grimme, *J. Comput. Chem.*, 2006, **27**, 1787–1799.

40 R. F. Bader, *Atoms in Molecules*, John Wiley & Sons, Ltd, New York, 1990.

41 G. Henkelman, A. Arnaldsson and H. Jónsson, *Comput. Mater. Sci.*, 2006, **36**, 354–360.

42 H. Jonsson, G. Mills and K. W. Jacobsen, in *Classical and Quantum Dynamics in Condensed Phase Simulations*, ed. B. J. Berne, G. Ciccotti and D. F. Coker, World Scientific, Singapore, 1998, p. 385.

43 Y. Liu, V. I. Artyukhov, M. Liu, A. R. Harutyunyan and B. I. Yakobson, *J. Phys. Chem. Lett.*, 2013, **4**, 1737–1742.

44 C. Ma, X. Shao and D. Cao, *J. Mater. Chem.*, 2012, **22**, 8911–8915.

45 D. Datta, J. Li and V. B. Shenoy, *ACS Appl. Mater. Interfaces*, 2014, **6**, 1788–1795.